ORIGINAL ARTICLE

Comparison of Taiwanese and European Calibration Factors for Heart-to-Mediastinum Ratio in Multicenter ^{123}I-mIBG Phantom Studies

Koichi Okuda[1), 2)], Kenichi Nakajima[3)], Guang-Uei Hung[4)], Hao-Ting Wu[4)], Derk O. Verschure[5), 6)], Hein J. Verberne[5)], and Chiemi Kitamura[7)]

Received: June 21, 2023/Revised manuscript received: August 31, 2023/Accepted: September 1, 2023

Abstract

***Background*: Cross-calibration of ^{123}I-labeled *meta*-iodobenzylguanidine (*m*IBG) myocardial-derived indices is essential to extrapolate findings from several clinical centers. Here, we conducted a phantom study to generate conversion coefficients for the calibration of heart-to-mediastinum ratios and compare them between Taiwan and Europe.**

***Methods*: We used an acrylic phantom dedicated to ^{123}I-*m*IBG planar imaging to calculate the conversion coefficients of 136 phantom images derived from 36 Taiwanese institutions. A European phantom image database including 191 images from 27 institutions was used. Conversion coefficients were categorized into five collimator types: low-energy (LE) high-resolution (LEHR), LE general-purpose (LEGP), extended LEGP (ELEGP), medium-energy (ME) GP (MEGP), and ME low-penetration (MELP) collimators.**

***Results*: The conversion coefficients were 0.53 ± 0.039, 0.59 ± 0.032, 0.79 ± 0.032, 0.96 ± 0.038, and 0.99 ± 0.050 for LEHR, LEGP, ELEGP, MEGP, and MELP collimators, respectively. The Taiwanese and European conversion coefficients for the LEHR, LEGP, and MELP collimators did not significantly differ. The coefficient of variation was slightly higher for the Taiwanese than the European conversion coefficients (3.7%–7.5% *vs.* 2.3%–5.6%).**

***Conclusions*: We calculated conversion coefficients for various types of collimators used in Taiwan using a ^{123}I-*m*IBG phantom. In general, the Taiwanese and European conversion coefficients were comparable. These findings further corroborated and highlighted the need for ^{123}I-*m*IBG standardization using the phantom-determined conversion coefficients.**

Keywords: ^{123}I-*m*IBG, Calibration, Collimator, Heart-to-mediastinum ratio, Phantom

Ann Nucl Cardiol 2023; 9 (1): 54–60

Cardiac sympathetic nerve activity has been visualized using the noradrenaline analogue ^{123}I-labeled *m*eta-iodobenzylguanidine (*m*IBG) (1, 2), and ^{123}I-*m*IBG cardiac scintigraphy is now established for the diagnostic evaluation of heart failure (3–5) and neurodegenerative diseases (6–10). The heart-to-mediastinum ratio (HMR) is calculated as the ratio of ^{123}I-*m*IBG average counts in the heart to those in the mediastinum to semi-quantify cardiac sympathetic nerve activity from ^{123}I-*m*IBG images (11, 12). The HMR also plays an important clinical role in both cardiology and neurology.

We previously showed that the HMR is significantly impacted by collimator types (13–16). Consequently, we

DOI: 10.17996/anc.23-00006

1) Department of Radiation Science, Hirosaki University Graduate School of Health Sciences, Aomori, Japan
2) Department of Physics, Kanazawa Medical University, Ishikawa, Japan
3) Department of Functional Imaging and Artificial Intelligence, Graduate School of Advanced Preventive Medical Sciences, Kanazawa University, Ishikawa, Japan
4) Department of Nuclear Medicine, Chang Bing Show Chwan Memorial Hospital, Changhua, Taiwan
5) Department of Radiology and Nuclear Medicine, Amsterdam University Medical Centers, University of Amsterdam, Amsterdam, The Netherlands
6) Department of Cardiology, Zaans Medical Center, Zaandam, The Netherlands
7) PDRadiopharma Inc., Tokyo, Japan

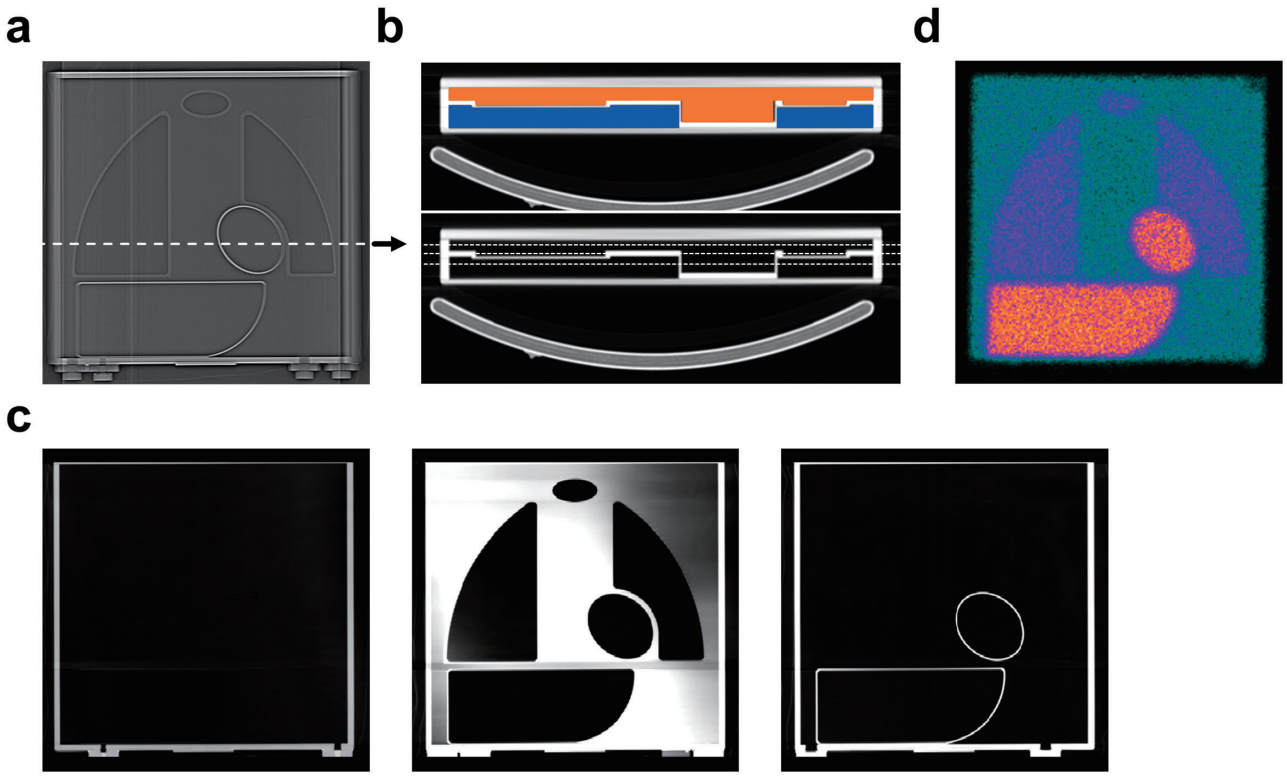

Figure 1 Structure of ^{123}I-*m*IBG phantom consisting of two compartments.
a: X-ray CT scout view of anterior ^{123}I-*m*IBG phantom.
b: Transaxial phantom image of central scout view shows one compartment each for radionuclide (orange) and water (blue).
c: Upper (left), middle (center), and bottom (right) layers of ^{123}I-*m*IBG phantom in transaxial phantom image.
d: Sample image of anterior ^{123}I-*m*IBG phantom with medium-energy collimator.

devised a means of HMR cross-calibration based on the characteristics of various collimators (17–21) that could convert and unify all HMRs as though they were derived from a single standard type (i.e., medium energy [ME] collimator). The HMR standardization method is based on an acrylic chest phantom that was designed for ^{123}I-*m*IBG planar imaging (13). We validated this method in multicenter phantom studies in Japan and Europe (22). However, some small discrepancies in calibration factors between the two studies could be explained by types of phantoms. Japanese and European data were acquired using one (13)-, and two (21)- compartment phantoms for radionuclides only and radionuclides and water, respectively. These discrepancies could also be explained by differences in specific collimator and gamma camera combinations.

We therefore conducted a multi-center ^{123}I-*m*IBG phantom study in Taiwan to obtain and confirm the distribution of calibration factors determined in Europe using two-compartment phantoms.

Material and methods

Calibration phantom for planar ^{123}I-*m*IBG imaging

We calibrated HMRs under various collimator imaging conditions using a flat, polymethyl methacrylate phantom (Hokuriku Yuuki Industry, Co., Ltd., Kanazawa, Japan) measuring 396 w × 386 d × 50 h mm^3 (Figure 1) (22). This phantom can mimic planar ^{123}I-*m*IBG distribution in the heart, mediastinum, liver, lungs, and thyroid gland. Planar images were acquired from the phantom containing 111 MBq of ^{123}I-*m*IBG. Anterior and posterior planar ^{123}I-*m*IBG images were acquired from both sides of the phantom. The theoretical HMRs after decay correction of anterior and posterior views were 2.60 and 3.50, respectively.

Quantitative analysis of ^{123}I-*m*IBG images

The HMR was calculated as cardiac ^{123}I-*m*IBG uptake divided by ^{123}I-*m*IBG background activity in the upper mediastinal region. Circular and rectangular regions of interest (ROIs) were automatically delineated on the heart and mediastinum, respectively, using a fully automated algorithm, called smartPhantom (Supplementary Figure 1). The ROI sizes and positions were determined by using templates at the heart and mediastinum based on smartMIBG software (23).

Calibration factor for HMR in gamma camera and collimator system

A calibration factor was calculated from the HMR derived from anterior (HMR_{Ant}) and posterior (HMR_{Post}) planar ^{123}I-

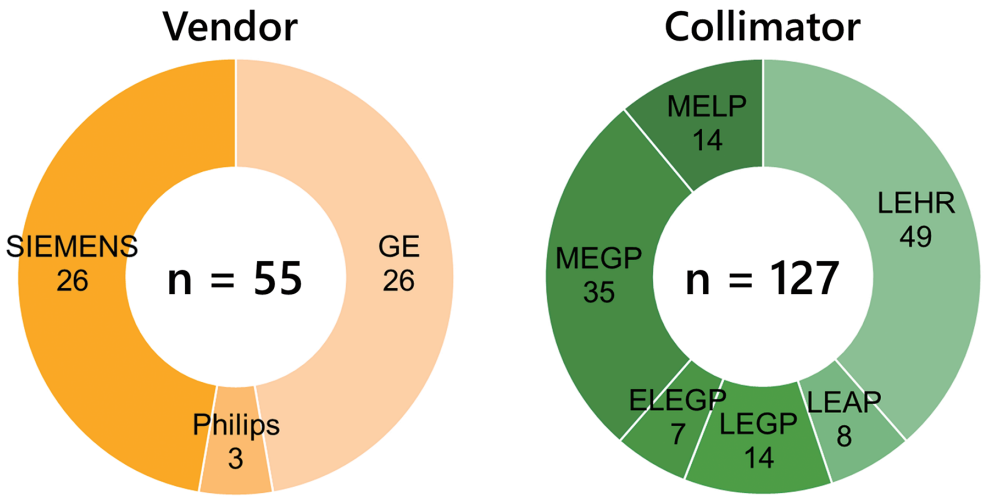

Figure 2 Numbers of gamma cameras and collimators used in Taiwanese ^{123}I-*m*IBG phantom study.
ELEGP, extended low-energy general-purpose; LEAP, low-energy all-purpose; LEGP, low-energy general-purpose; LEHR, low-energy high-resolution; LMEGP, low-medium-energy general-purpose; MEGP, medium-energy general-purpose; MELP, ME low-penetration.

*m*IBG phantom images using smartMIBG algorithm. Conversion coefficients were calculated as:

Conversion coefficient = ([HMR_{Ant} + HMR_{Post}] /2 -1)/ ([2.60 + 3.50] /2 -1)

, where 2.60 and 3.50 are the respective designated HMRs in anterior and posterior views of the calibration phantom.

Multicenter ^{123}I-*m*IBG phantom study in Taiwan

We obtained 136 phantom image sets generated by 36 institutions in Taiwan (Appendix) between June 2021 and May 2022 using four gamma camera manufacturers (GE Healthcare, Waukesha, WI, USA; Philips Healthcare, Milpitas, CA, USA; Siemens Healthineers, Erlangen, Germany, and Spectrum Dynamics Medical, Caesarea, Israel). We focused on the more popular collimators: low-energy (LE) high-resolution (LEHR), LE all-purpose (LEAP), LE general-purpose (LEGP), extended LEGP (ELEGP), medium energy GP (MEGP), and ME low-penetration (MELP). We excluded five phantom images acquired using specific and rarely used/available collimators: LE high-resolution-sensitivity (n=1), high-energy GP (n=3) by GE Healthcare, and LPHR (n=1) by Siemens Healthineers. We also excluded D-SPECT by Spectrum Dynamics Medical, NM 530c, NM/CT 670 CZT, and NM/CT 870 CZT by GE Healthcare due to difficulties acquiring planar images from CZT-based systems. Planar images were acquired with a 256 × 256 matrix and the photopeak window of ^{123}I centered at 159 keV with a 20% energy window. All images were acquired for 120 sec except for those from one institution, where the duration was 180 sec. Pixel sizes were 2.21, 2.33, and 2.4 mm for GE, Philips, and Siemens instruments, respectively.

European phantom image datasets

We validated the conversion coefficients of the Taiwanese datasets using those of European ^{123}I-*m*IBG phantom images (22). The European studies proceeded in 27 institutions in Austria, Belgium, the Netherlands, and United Kingdom. The phantom images were acquired using LEHR (n=100), LEGP (n=10), MEGP (n=28), and MELP (n=53) collimators. The anterior and posterior planar images were acquired with a 256 ×256 matrix. The photopeak window of ^{123}I was centered at 159 keV with a 15% energy window. The acquisition duration was 300 sec. Pixel sizes were 2.21, 2.33, and 2.40 mm for GE Healthcare, Philips, and Siemens Healthineers instruments, respectively.

Statistical analysis

Continuous values are expressed as means ± SD. Normality in the continuous dataset was evaluated using Shapiro-Wilk tests. Differences in continuous variables were analyzed using Student t-tests and Wilcoxon signed-rank tests. Coefficients of variation (CV) were calculated as standard deviation divided by the mean. All statistical tests were two-tailed, and values with $p<0.05$ were considered significant. All data were statistically analyzed using JMP version 11.2.1 (SAS Institute Inc., Cary, NC, USA).

Results

We examined phantom images acquired using 55 gamma cameras and 127 collimators (Figure 2). Since the collimator performance of LEAP and LEGP were similar, conversion coefficients derived from both collimators were combined. Conversion coefficients were calculated for LEHR (n=49), LEGP (n=22), ELEGP (n=7), MEGP (n=35), and MELP (n=

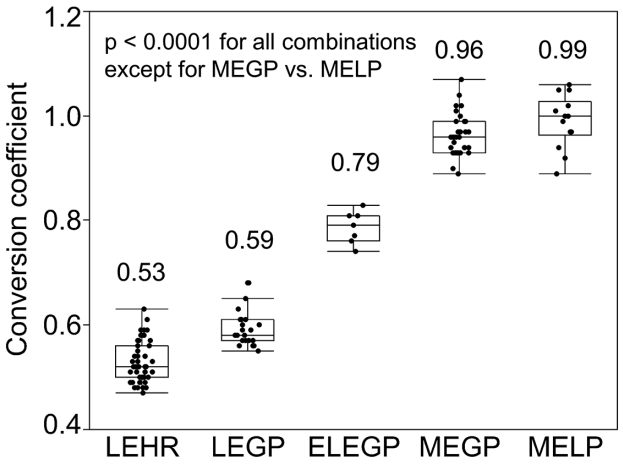

Figure 3 Distribution of conversion coefficients in LEHR, LEGP, ELEGP, MEGP, and MELP collimators.

14) collimators. The distribution of conversion coefficients was collimator dependent, being 0.53 ± 0.039, 0.59 ± 0.032, 0.79 ± 0.032, 0.96 ± 0.038, and 0.99 ± 0.050 for LEHR, LEGP, ELEGP, MEGP, and MELP, respectively (Figure 3). The conversion coefficients for MEGP and MELP collimators did not significantly differ. The conversion coefficients derived from three manufacturers did not differ in LEHR, LEGP, and MEGP collimators. (Supplementary Table 1). The Taiwanese and European conversion coefficients for LEHR, LEGP, and MELP collimators also did not significantly differ (Figure 4), whereas those for MEGP collimators were significantly lower (0.96 ± 0.035 *vs.* 0.99 ± 0.023; p<0.001). Moreover, the difference remained when the conversion coefficients for MEGP and MELP collimators were combined (Taiwan *vs.* Europe: 0.97 ± 0.042 *vs.* 1.00 ± 0.034; p<0.001). The CVs were smaller for LEHR, LEGP, MEGP, and MELP in Europe than in Taiwan, being respectively, 4.6% *vs.* 7.5%, 5.6% *vs.* 5.8%, 2.3% *vs.* 3.7%, and 3.7% *vs.* 5.0%.

Discussion

The major findings of the present study were that Taiwanese multicenter ^{123}I-*m*IBG phantom-derived conversion coefficients differed according to collimator type, and were comparable to those in Europe.

The Japanese multicenter ^{123}I-*m*IBG phantom study was completed before the European and Taiwanese studies (19), and we found higher conversion coefficients in Taiwan and Europe than in Japan. This was because a conventional, single-compartment ^{123}I-*m*IBG phantom was used in Japan (13), whereas modified light-weight two-compartment ^{123}I-*m*IBG phantoms were used in Taiwan and Europe (22). The Japanese conversion coefficients (n = 597) correlated with those in Taiwan and Europe (n = 322). Therefore, we generated a regression line of mean conversion coefficients (Supplementary Figure 2) that might facilitate cross-calibration among Japan, Taiwan, and Europe.

Since similar modified light-weight phantoms were used in Taiwan and Europe, conversion coefficients were equivalent in popular collimators. The difference in mean conversion coefficients for the MEGP collimators between Taiwan and Europe was quite small, but significant. In addition, the CV of the conversion coefficients tended to be smaller for the European than the Taiwanese data. Moreover, Taiwanese conversion coefficient was computed from three manufacturers, while European data was from two (Supplementary Table 2). Several factors influence conversion coefficients during ^{123}I-*m*IBG imaging, such as the primary energy window setting (17). The energy windows were 159% ± 7.5% and 159% ± 10% keV in the European and Taiwanese studies, respectively. The amount of ^{123}I activity was higher in Taiwan than in Europe (185 *vs.* 111 MBq), and the acquisition time was longer in Europe than in Taiwan (5 *vs.* 2 min). However, the effects on the converted HMRs were relatively small due to differences in the conversion coefficients. If an HMR of 1.7 acquired under LEGP conditions (conversion coefficient=0.59 in common with two areas) was converted to Taiwanese and European MEGP (conversion coefficients = 0.96 and 0.99, respectively), the converted HMR values of 2.14 (Taiwan) and 2.17 (Europe) were equivalent. The converted HMRs were calculated as conversion coefficients under MEGP/divided by those under LEGP × (unconverted HMR - 1) + 1 (19).

Low-medium energy (LME) collimators are advantageous for nuclear cardiology because various isotopes that are routine in the Japanese clinical setting such as ^{201}Tl, ^{99m}Tc, and ^{123}I can be selected. Although LEHR and LEGP collimators are suitable for ^{201}Tl and ^{99m}Tc, 529 keV photons emitted by ^{123}I can easily penetrate the thin septa of these collimators, thus degrading ^{123}I-*m*IBG planar images. In contrast, MEGP and MELP collimators take high-energy photons into account and are more suitable for ^{123}I-*m*IBG imaging. The LME collimators, such as ELEGP and LMEGP, can also reduce the effect of high energy photons, while still being applicable to ^{201}Tl and ^{99m}Tc imaging. However, the LMEGP collimator is not commercially available in Taiwan.

The standardization of HMR is essential for clinical evaluations of cardiac ^{123}I-*m*IBG uptake among clinical centers. The conversion coefficients varied among all five, and significantly differed between collimator groups. Based on these results, we suggest that all HMRs should be standardized using conversion coefficients derived from a dedicated phantom. Moreover, since ME collimators are preferred in the clinical imaging guidelines published by the American Society of Nuclear Cardiology (24) and in the proposal for standardizing ^{123}I-*m*IBG cardiac imaging by the Cardiovascular Committee of the European Association of Nuclear Medicine and the European Council of Nuclear Cardiology

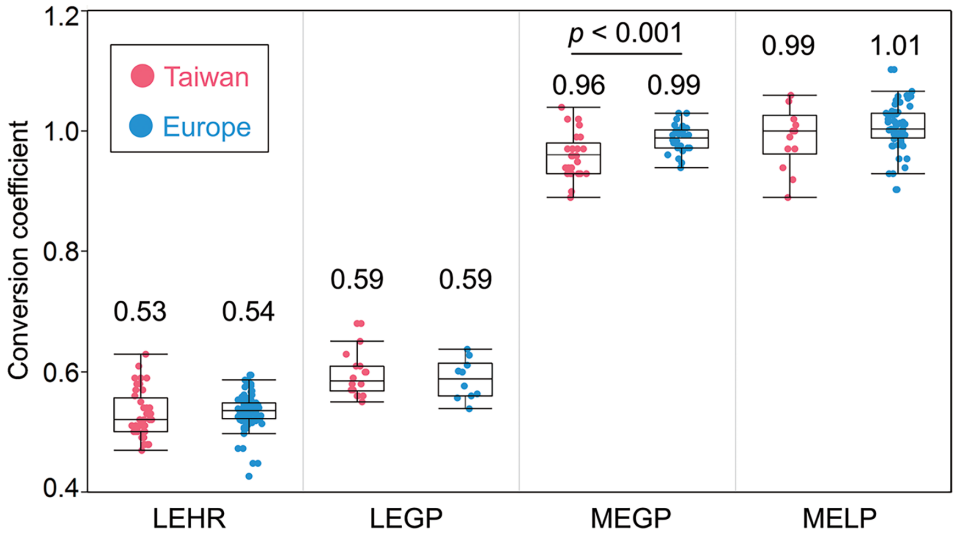

Figure 4 Distribution of conversion coefficients in Taiwanese (red) and European (blue) ^{123}I-*m*IBG phantom studies.

(25), we decided to standardize all HMR values to ME collimator conditions.

Our study is limited by our focus on conversion coefficient comparisons between Taiwan and Europe. We also did not compare potential differences in clinical outcomes. However, harmonizing HMR values for differences in collimators and gamma cameras is conceivable and would unify the prognostic potential of ^{123}I-*m*IBG cardiac imaging on a global scale. In fact, clinical implications in Japan have already been published (17–19). Consequently, conversion coefficients in general, irrespective of geographical location, should result in HMRs with comparable clinical impact. We excluded the phantom images derived from the CZT camera system. Since the D-SPECT system could generate a planogram equivalent to a planar anterior image, our research group developed the methodology to compare Anger and CZT cameras by calculating the conversion coefficients (26). Recently, we validated the methodology in 173 patients with neurodegenerative disease and heart failure (27). In the near future, standardization of HMR using conversion factors could be implemented in both Anger and CZT cameras.

Conclusions

Our ^{123}I-*m*IBG cross-calibration phantom enabled us to generate conversion coefficients in accordance with collimator performance that were equivalent between Taiwanese and European multicenter data. International studies using standard HMRs should be conducted using conversion coefficients derived from a dedicated ^{123}I-*m*IBG phantom.

Acknowledgments

We thank the physicians, technologists, and colleagues who participated in this study. The authors appreciate editorial assistance provided by Norma Foster.

K.O. drafted the manuscript and K.N., G.H., D.V., H.V., and C.K. edited it. K.O., K.N. G.H. performed data analysis and interpretation. K.O. performed the statistical analysis of the data and K.N. confirmed it. G.H., H.W., D.V., H.V., and C.K. corrected multicenter phantom image datasets.

Sources of funding

This work was supported in part by JSPS KAKENHI (Grant No: 18K15649, PI Koichi Okuda), JSPS KAKENHI (C) (Grant No: 23K07203, PI: Kenichi Nakajima), and the National Science and Technology Council of Taiwan (Grant No: 110-2623-E-758-001-NU, PI: Guang-Uei Hung).

Conflicts of interest

K. Nakajima and K. Okuda collaborate with PDRadiopharma Inc., Tokyo, Japan, and K. Nakajima belongs to an endowed department partly funded by PDRadiopharma Inc. C. Kitamura is an employee of PDRadiopharma Inc., Tokyo, Japan.

Reprint requests and correspondence 1:
Koichi Okuda, PhD
Department of Radiation Science, Hirosaki University Graduate School of Health Sciences. 66-1 Hon-cho, Hirosaki-shi, Aomori 036-8564, Japan
E-mail: okuda1@hirosaki-u.ac.jp
Correspondence 2:
Guang-Uei Hung, MD
Department of Nuclear Medicine, Chang Bing Show Chwan Memorial Hospital, No. 6, Lukong Road, Lukang Town, Changhua 505, Taiwan
E-mail: 106143@gmail.com

Appendix

Participating institutions in Taiwan

Asia University Hospital (Taichung)
Buddhist Tzu Chi Medical Foundation Dalin Tzu Chi Hospital (Dalin)
Buddhist Tzu Chi Medical Foundation Taichung Tzu Chi Hospital (Taichung)
Chang Bing Show Chwan Hospital (Lukang)
Chang-Geng Medical Foundation Chiayi Chang-Geng Memorial Hospital (Puzi)
Chang-Geng Medical Foundation Linkou Chang-Geng Memorial Hospital (Taoyuan)
Changhua Christian Hospital (Changhua)
Cheng Ching Hospital (Taichung)
China Medical University Hospital (Taichung)
China Medical University Hsinchu Hospital (Zhubei)
Chung Shan Medical University Hospital (Taichung)
Da Chien General Hospital (Miaoli)
Far Eastern Memorial Hospital (New Taipei)
Feng Yuan Hospital (Taichung)
Fu Jen Catholic University Hospital (New Taipei)
Jen-Ai Hospital (Taichung)
Kaohsiung Medical University Chung-Ho Memorial Hospital (Kaohsiung)
Kaoshiung Chang Gung Memorial Hospital (Kaohsiung)
Keelung Chang Gung Memorial Hospital (Keelung)
Koo Foundation Sun Yat-Sen Cancer Center (Taipei)
Landseed International Hospital (Taoyuan)
Lin Shin Hospital (Taichung)
Nantou Hospital, Ministry of Health and Welfare (Nantou)
National Cheng Kung University Hospital (Tainan)
National Taiwan University Cancer Center (Taipei)
National Taiwan University Hospital (Taipei)
NTU BioMedical Park Hospital (Taipei)
Saint Paul's Hospital (Taoyuan)
Shin Kong Wu Ho-Su Memorial Hospital (Taipei)
Show Chwan Memorial (Taipei)
Taichung Veterans General Hospital (Taichung)
Tainan Sin-Lau Hospital (Tainan)
Taipei City Hospital Heping Renai Branch (Taipei)
Taipei Medical University Hospital (Taipei)
Taipei Veterans General Hospital (Taipei)
Tri-Service General Hospital (Taipei)

References

1. Wieland DM, Brown LE, Rogers WL, et al. Myocardial imaging with a radioiodinated norepinephrine storage analog. J Nucl Med 1981; 22: 22–31.
2. Schofer J, Spielmann R, Schuchert A, Weber K, Schlüter M. Iodine-123 meta-iodobenzylguanidine scintigraphy: A non-invasive method to demonstrate myocardial adrenergic nervous system disintegrity in patients with idiopathic dilated cardiomyopathy. J Am Coll Cardiol 1988; 12: 1252–8.
3. Nakata T, Nakajima K, Yamashina S, et al. A pooled analysis of multicenter cohort studies of ^{123}I-*m*IBG imaging of sympathetic innervation for assessment of long-term prognosis in heart failure. JACC Cardiovasc Imaging 2013; 6: 772–84.
4. Verschure DO, Veltman CE, Manrique A, et al. For what endpoint does myocardial 123I-MIBG scintigraphy have the greatest prognostic value in patients with chronic heart failure? Results of a pooled individual patient data meta-analysis. Eur Heart J Cardiovasc Imaging 2014; 15: 996–1003.
5. Travin MI, Matsunari I, Thomas GS, Nakajima K, Yoshinaga K. How do we establish cardiac sympathetic nervous system imaging with ^{123}I-*m*IBG in clinical practice? Perspectives and lessons from Japan and the US. Ann Nucl Cardiol 2019; 5: 5–20.
6. Orimo S, Suzuki M, Inaba A, Mizusawa H. ^{123}I-MIBG myocardial scintigraphy for differentiating Parkinson's disease from other neurodegenerative parkinsonism: A systematic review and meta-analysis. Parkinsonism Relat Disord 2012; 18: 494–500.
7. Treglia G, Cason E, Stefanelli A, et al. MIBG scintigraphy in differential diagnosis of Parkinsonism: A meta-analysis. Clin Auton Res 2012; 22: 43–55.
8. Yoshita M, Arai H, Arai H, et al. Diagnostic accuracy of ^{123}I-meta-iodobenzylguanidine myocardial scintigraphy in dementia with Lewy bodies: A multicenter study. PLoS One 2015; 10: e0120540.
9. Komatsu J, Samuraki M, Nakajima K, et al. ^{123}I-MIBG myocardial scintigraphy for the diagnosis of DLB: A multicentre 3-year follow-up study. J Neurol Neurosurg Psychiatry 2018; 89: 1167–73.
10. Yamada M, Komatsu J, Nakamura K, et al. Diagnostic criteria for dementia with Lewy bodies: Updates and future directions. J Mov Disord 2020; 13: 1–10.
11. Merlet P, Valette H, Dubois-Randé JL, et al. Prognostic value of cardiac metaiodobenzylguanidine imaging in patients with heart failure. J Nucl Med 1992; 33: 471–7.
12. Veltman CE, Boogers MJ, Meinardi JE, et al. Reproducibility of planar ^{123}I-meta-iodobenzylguanidine (MIBG) myocardial scintigraphy in patients with heart failure. Eur J Nucl Med Mol Imaging 2012; 39: 1599–608.
13. Nakajima K, Matsubara K, Ishikawa T, et al. Correction of iodine-123-labeled meta-iodobenzylguanidine uptake with multi-window methods for standardization of the heart-to-mediastinum ratio. J Nucl Cardiol 2007; 14: 843–51.
14. Verberne HJ, Feenstra C, de Jong WM, Somsen GA, van Eck-Smit BLF, Busemann Sokole E. Influence of collimator choice and simulated clinical conditions on ^{123}I-MIBG heart/mediastinum ratios: A phantom study. Eur J Nucl Med Mol Imaging 2005; 32: 1100–7.
15. Dobbeleir AA, Hambÿe AS, Franken PR. Influence of high-energy photons on the spectrum of iodine-123 with low- and medium-energy collimators: consequences for imaging with ^{123}I-labelled compounds in clinical practice. Eur J Nucl Med 1999; 26: 655–8.
16. Inoue Y, Suzuki A, Shirouzu I, et al. Effect of collimator choice on quantitative assessment of cardiac iodine 123 MIBG uptake. J Nucl Cardiol 2003; 10: 623–32.

17. Okuda K, Nakajima K, Kitamura C, Kirihara Y, Hashimoto M, Kinuya S. Calibrated scintigraphic imaging procedures improve quantitative assessment of the cardiac sympathetic nerve activity. Sci Rep 2020; 10: 21834.
18. Nakajima K, Okuda K, Matsuo S, et al. Standardization of metaiodobenzylguanidine heart to mediastinum ratio using a calibration phantom: Effects of correction on normal databases and a multicentre study. Eur J Nucl Med Mol Imaging 2012; 39: 113–9.
19. Nakajima K, Okuda K, Yoshimura M, et al. Multicenter cross-calibration of I-123 metaiodobenzylguanidine heart-to-mediastinum ratios to overcome camera-collimator variations. J Nucl Cardiol 2014; 21: 970–8.
20. Nakajima K, Okuda K, Matsuo S, Agostini D. The time has come to standardize ^{123}I-MIBG heart-to-mediastinum ratios including planar and SPECT methods. Eur J Nucl Med Mol Imaging 2016; 43: 386–8.
21. Nakajima K, Verschure DO, Okuda K, Verberne HJ. Standardization of ^{123}I-*meta*-iodobenzylguanidine myocardial sympathetic activity imaging: Phantom calibration and clinical applications. Clin Transl Imaging 2017; 5: 255–63.
22. Verschure DO, Poel E, Nakajima K, et al. A European myocardial ^{123}I-mIBG cross-calibration phantom study. J Nucl Cardiol 2018; 25: 1191–7.
23. Okuda K, Nakajima K, Hosoya T, et al. Semi-automated algorithm for calculating heart-to-mediastinum ratio in cardiac Iodine-123 MIBG imaging. J Nucl Cardiol 2011; 18: 82–9.
24. Henzlova MJ, Duvall WL, Einstein AJ, Travin MI, Verberne HJ. ASNC imaging guidelines for SPECT nuclear cardiology procedures: Stress, protocols, and tracers. J Nucl Cardiol 2016; 23: 606–39.
25. Flotats A, Carrió I, Agostini D, et al. Proposal for standardization of ^{123}I-metaiodobenzylguanidine (MIBG) cardiac sympathetic imaging by the EANM Cardiovascular Committee and the European Council of Nuclear Cardiology. Eur J Nucl Med Mol Imaging 2010; 37: 1802–12.
26. Nakajima K, Okuda K, Yokoyama K, et al. Cross calibration of ^{123}I-meta-iodobenzylguanidine heart-to-mediastinum ratio with D-SPECT planogram and Anger camera. Ann Nucl Med 2017; 31: 605–15.
27. Yamashita S, Nakajima K, Okuda K, et al. Phantom-based standardization method for ^{123}I-meta-iodobenzylguanidine heart-to-mediastinum ratio validated by D-SPECT versus Anger camera. Ann Nucl Cardiol 2023; epub a head of print. DOI: 10.17996/anc.23-00003